Vol 15 No 3, March 2006
1009-1963/2006/15(03)/0556-06
Chinese Physics
© 2006 Chin. Phys. Soc.
and IOP Publishing Ltd

Analyses of edge plasma characteristics in HL-2A

Hong Wen-Yu(洪文玉)†, Yan Long-Wen(严龙文), Qian Jun (钱 俊),
Pan Yu-Dong(潘宇东), Wang En-Yao(王恩耀), Luo Cui-Wen(罗翠文),
Xu Zheng-Yu(徐征宇), Pan Li(潘 莉), Li Qiang(李 强),
Yuan Bao-Shan(袁保山), Liu Li(刘 莉), and Ding Xuan-Tong(丁玄同)

Southwestern Institute of Physics, Chengdu 610041, China

(Received 9 May 2005; revised manuscript received 8 October 2005)

The edge plasma characteristics are studied by both a movable array of Mach/Reynolds stress/Langmuir 10-probes in the boundary region and the fixed flush probe arrays on the 4 divertor neutralization plates at the same toroidal cross-section in the HL-2A tokamak. The dependence of the Reynolds stress on poloidal flow in the edge plasma is analysed. The result indicates that the sheared poloidal flow in tokamak plasma can be induced by the radial gradient of Reynolds stress. In the divertor experiments of HL-2A, the profiles of the electron temperature, density and floating potential on divertor plates are measured by the flush probe arrays. The edge electron temperature in divertor configuration is higher than that in limiter configuration. The temperature asymmetry between outer and inner target plates is observed. The result of magnetic surface reconstructed from 18 Mirnov coils signals is presented. Both the particle recycling and the impurity flux in the bulk plasma during divertor discharges are discussed. Neutral gas pressure in divertor chamber, measured by fast ionization gauge during divertor discharge, is given.

Keywords: HL-2A tokamak, divertor configuration, movable probe array, flush probe array
PACC: 5230, 5235R, 5255G

1. Introduction

HL-2A tokamak is a fusion research device with double-null divertors. It provides better experimental conditions to investigate edge plasma features, such as confinement performance, particle and impurity behaviours, power deposition and material erosion. Particularly, impurity product and transport due to plasma surface interaction may be effectively controlled by the divertor. The charge state and energy of the ion flux incident upon limiter or divertor plate surface are the most important sources to produce the impurities by physical and chemical sputterings. The latter also depends on the surface material and temperature. The impurity transport depends strongly on scrape-off layer (SOL) plasma parameters, such as temperature, density, transport coefficients and flow velocity. A basic goal for the control of particle and impurity is to remove the products of the fusion reaction and to avoid excessive contamination of core plasma.

Ion collision can lead to an increase in impurity sputtering from narrow divertor entry components. Compared with the impurity from the neutralization plate, the impurities from the divertor entry can greatly contaminate the core plasma. Consequently, one of main objectives for the divertor experiments is to pump the particles and impurities produced from the divertor entry components and its target plate.[1−4] The profiles of the boundary temperature and the density in HL-2A are measured by both a movable probe array located in the midplane and the flush probe arrays in the divertor chamber. They provide parameters important to analysing edge plasma characteristics.

2. Measurement principle of Langmuir electrostatic probes

The edge plasma parameters along the HL-2A midplane are measured by a Mach/Reynolds stress/Langmuir probe array with 10 pins assembly mounted on the same graphite probe seat, as shown in Fig.1. Pins 1–2 act as a Mach probe to collect ion saturation current in the poloidal direction. Pins 3–6 consist of the Reynolds stress probe.[5] They are

†Corresponding author. E-mail: hongwy@swip.ac.cn

used to measure floating potential and then calculate the radial and poloidal electric field fluctuations. Pins 7–10 consist of the four Langmuir probes. The probe array assembly is mounted on a long shaft, which can be moved radially and rotated through 360° around the shaft axis. These probes can measure edge plasma temperature, density, poloidal electric field, radial electric field, Reynolds stress, poloidal rotation velocity and their profiles obtained by changing the radial position of the probe array in different discharges. Measured results can provide the information on plasma confinement, turbulent fluctuations and their correlation.

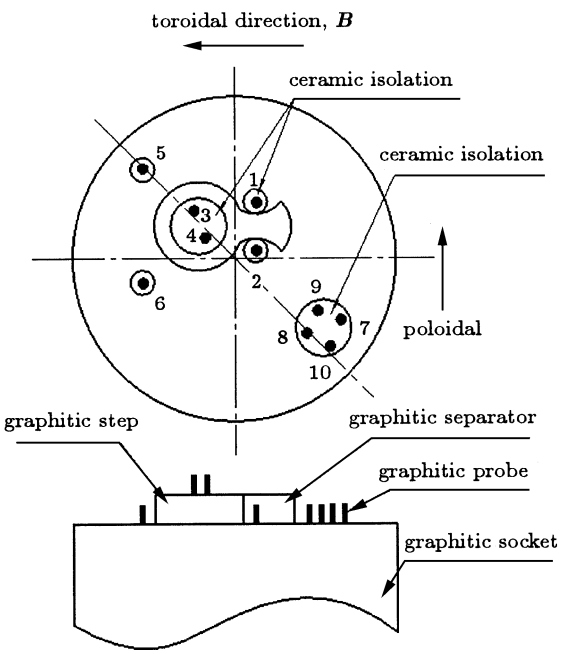


Fig.1. The arrangement of the Mach/Reynolds stress/Langmuir 10-probe array in HL-2A.

Four arrays of Langmuir probes are installed onto the inner and outer neutralization plates of both upper and lower divertor on the HL-2A tokamak, separately. Each neutralization plate is perpendicular to the midplane. Each array is composed of seven groups of probes with 3 flush pins, each with a thickness of 10mm, located at the same toroidal angle, as shown in Fig.2. The magnetic field is incident upon the probe surfaces at an angle of about 2°. Flush probe has very long lifetime due to very low heat flux incident at small angle. Each pin top surface with 5mm in diameter and 6mm in height is parallel to the probe seat surface, and is referred to as flush probe.[5] Its spatial resolution is 10mm in vertical direction and 15mm in toroidal direction. The vertical positions of the flush probes in lower divertor are listed in Table 1. Figure 3 shows the orientation of flush probe array on target plate. The flush probes on neutralization plates can measure the profiles of the electron temperature, density and float potential. The profiles of energy or particle flow and their decay lengths can be estimated by the target temperature and density. They are very useful for investigating divertor physics.

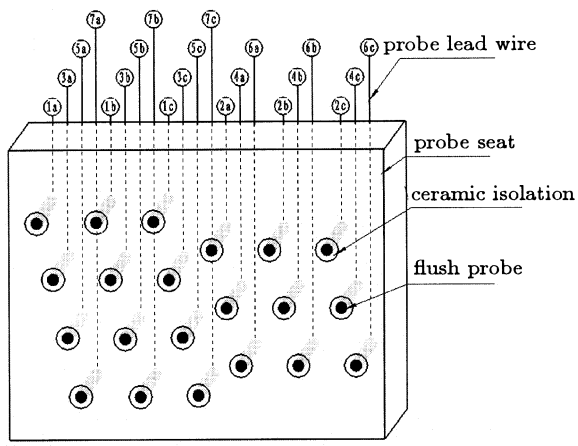


Fig.2. The arrangement of flush probe array.

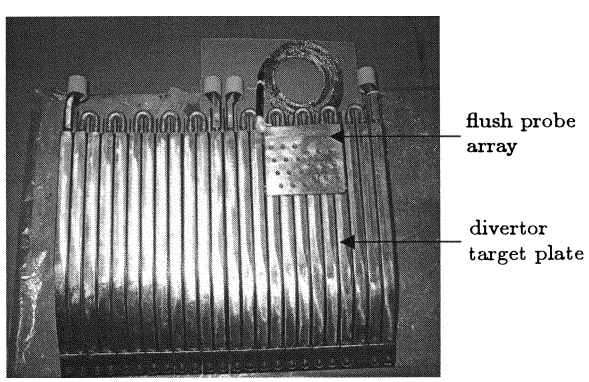


Fig.3. Orientation of flush probe array on target plate.

Table 1. The positions of flush probes on outer and inner neutralization plates in HL-2A.

Name	$R_{\text{outer}} = 163.5$cm							$R_{\text{inner}} = 139.5$cm						
Probe	T_{ed1}	T_{ed2}	T_{ed3}	T_{ed4}	T_{ed5}	T_{ed6}	T_{ed7}	T_{ed8}	T_{ed9}	T_{ed10}	T_{ed11}	T_{ed12}	T_{ed13}	T_{ed14}
Z/cm	–87	–86	–85	–84	–83	–82	–81	–86	–85	–84	–83	–82	–81	–80

The measurement circuit of electrostatic 4 probes is shown in Fig.4. If biased voltage between probe 1 and 2 satisfies $V_{\rm E} \gg kT_{\rm e}$, the edge electron temperature $T_{\rm ea}$, density $N_{\rm ea}$, space potential $V_{\rm s}$, poloidal electric field $E_{\rm p}$ or their profiles can be derived from ion saturation current $I_{\rm s}$ and respective potential differences as follows:

$$N_{\rm ea} = I_{\rm s}/(0.5Ae\sqrt{kT_{\rm e}/m_{\rm i}}), \tag{1}$$

$$T_{\rm ea} = 0.5 \times \varphi(V_3 + V_4 - 2V_{\rm f})/\ln 2, \tag{2}$$

$$V_{\rm s} = \varphi V_{\rm f} + \alpha T_{\rm ea}, \tag{3}$$

$$E_{\rm p} = \varphi(V_3 - V_4)/d_{34}, \tag{4}$$

$$\alpha = \frac{k}{e}\ln\left[2\pi\frac{m_{\rm e}}{m_{\rm i}}\left(Z + \frac{T_{\rm i}}{T_{\rm e}}\right)(1-\delta)^2\right], \tag{5}$$

where δ is the secondary electron emission yield of a probe, d_{34} is the poloidal distance between Probe 3 and 4, A is the effective collection area of the probe, and φ is the ratio of sampling resistance. The other parameters have usual physical meanings. For example H^+, when $T_{\rm i} = T_{\rm e}$ and $\delta = 0$, we obtain $\alpha = 2.49$. The poloidal velocity $V_{\rm pol}$ is estimated by[6−8]

$$V_{\rm pol} = J_{\rm pol}/en_{\rm e}. \tag{6}$$

Here $V_{\rm pol}$ is the poloidal flow velocity driven by the $\boldsymbol{E} \times \boldsymbol{B}$, $J_{\rm pol}$ and $n_{\rm e}$ are poloidal current density and electron density, respectively.

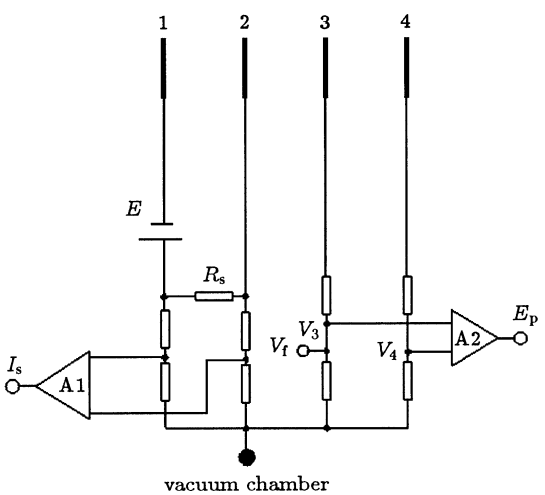


Fig.4. The measurement circuit of electrostatic 4 probes.

It has been known that the Reynolds stress can drive the poloidal rotation. When the contribution of magnetic fluctuation is neglected, the Reynolds stress $R_{\rm s}$ is determined by $R_{\rm s} = \langle\tilde{V}_r\tilde{V}_\theta\rangle$,[9−11] in which the $\langle\tilde{V}_r\tilde{V}_\theta\rangle$ term is related to the $\boldsymbol{E} \times \boldsymbol{B}$ drift velocity and defined as

$$\langle\tilde{V}_r\tilde{V}_\theta\rangle = -\langle\tilde{E}_r\tilde{E}_\theta\rangle/B^2, \tag{7}$$

where $\tilde{V}_r$ and $\tilde{V}_\theta$ are the radial and poloidal fluctuation flow velocities in edge plasma respectively, B is the toroidal magnetic field. The brackets $\langle\ldots\rangle$ refer to time average.

For a Mach/Reynolds stress probe array, the radial and poloidal electric field fluctuations $\tilde{E}_r$ and $\tilde{E}_\theta$ can be determined by,[11,12]

$$\tilde{E}_r = (\tilde{\phi}_{\rm f3} - \tilde{\phi}_{\rm f5})/r, \tag{8}$$

$$\tilde{E}_\theta = (\tilde{\phi}_{\rm f3} - \tilde{\phi}_{\rm f4})/\theta, \tag{9}$$

where $\tilde{\phi}_{\rm f}$ is the moment value of the float potential for the probe, r and θ are the radial and poloidal distances between 2 probes, respectively. All the data are sampled at 1 MHz with 12 bit resolutions by multichannel digitizer.

3. Results of edge plasma analyses

The design parameters in HL-2A are as follows: major radius R=1.64m, minor radius a=0.45m, plasma current $I_{\rm p}$=480kA, magnetic field $B_{\rm t}$=2.8T. In the first physics experiments, the achieved maximum parameters are $I_{\rm p}$=168kA, $B_{\rm t}$=1.4T, line-averaged density through central chord $n_{\rm e}(0)$=1.7×10^{19}m^{-3}, electron temperature $T_{\rm e0}$=0.4keV, discharge duration $t_{\rm pmax}$=920ms with a flattop time of about 500ms. The discharges with limiter configuration are first carried out. The limiter position can be scanned from 30cm to 45cm. The typical separatrix radii are 37cm–40cm for lower divertor discharges.

The edge parameters in the main plasma are measured by the movable probe array with 10 pins. Figure 5 shows the radial profiles of Reynolds stress and poloidal rotation velocity. The change of rotation velocity corresponds to that of Reynolds stress. This result supports that the radial gradient of Reynolds stress induced by edge plasma turbulence can drive poloidal flows. The radial profiles of edge electron temperature and density in limiter or divertor discharges are compared in Fig.6. The $T_{\rm ea}$ expresses the electron temperature in limiter discharge and $T_{\rm em}$ denotes the electron temperature in divertor discharge in Fig.6. In the discharges to analyse edge plasma feature, typical plasma parameters are $I_{\rm p}$=80–90kA, $B_{\rm t}$=1.2T, line-averaged density $n_{\rm e}(0)$=0.8×10^{19}m^{-3},

electron temperature T_{e0}=0.38keV, and discharge duration t_p=320ms with a flattop time of about 180ms, in the case of the movable limiter fixed at a=40cm. The edge electron temperatures in divertor discharges are 35% higher than those in limiter discharges, while corresponding electron densities in the divertor discharges are about 45% higher than those in the limiter discharges. These results confirm the fact that divertor discharge can improve plasma confinement. The temperature asymmetry between outer and inner target plates is analysed.

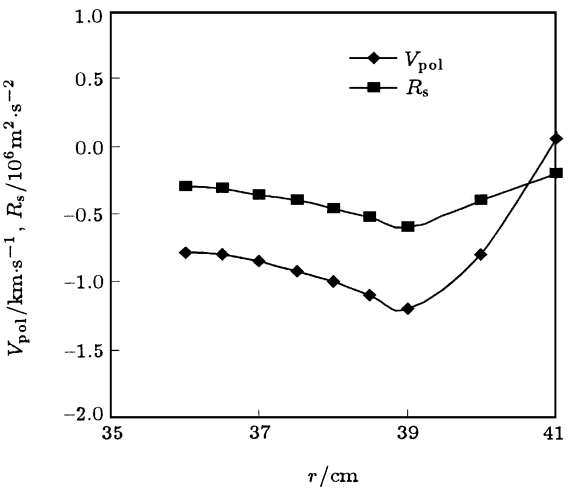


Fig.5. The radial profiles of poloidal rotation velocity V_{pol} and electrostatic Reynolds stress R_s during ohmic discharges.

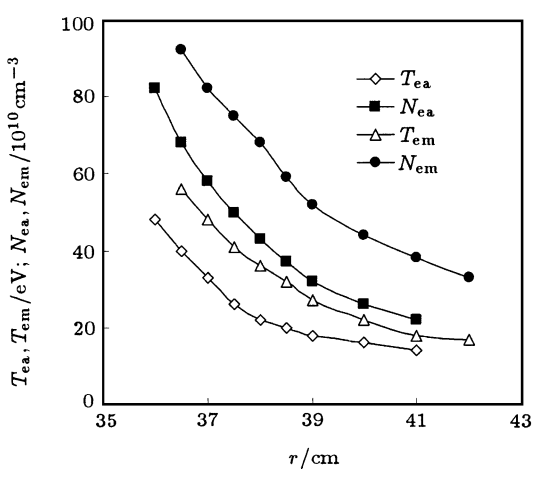


Fig.6. Radial profiles of edge electron temperatures and densities. The edge temperature T_{ea} and density N_{ea} with the movable limiter fixed at a radius of 40cm, the edge temperature T_{em} and densityN_{em} with both the divertor configuration, and the limiter fixed at a radius of 45cm.

Figure 7 presents the profiles of the electron temperature and density on divertor target plates during lower divertor discharges. The symbols of T_{ed} (LI), T_{ed} (LO), N_{ed} (LI) and N_{ed} (LO) represent the electron temperatures and densities on inner and outer target plates, respectively. The peak temperature on the outer target plate is about 60eV, 30% higher than that on the inner target plate. The decay length of the electron temperature is about 2 cm in private region. It is larger than 4 cm in SOL region. The peak density on the outer target is about one ninth of the line-averaged density in the main plasma. It is lower than that on the inner target. These results are roughly consistent with the predictions by theoretical models.

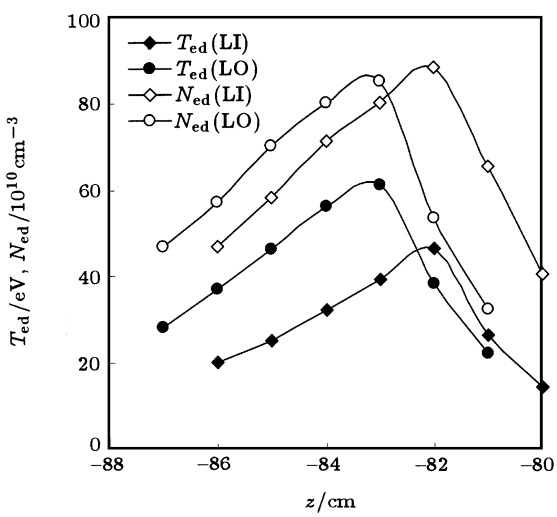


Fig.7. The target profiles of electron temperature and density. The electron temperature T_{ed} and density N_{ed} on the outer (LO) and inner (LI) target plates for lower divertor

Figure 8 shows the time evolutions of the plasma current (I_p), edge electron temperature at mid-plane radius r=40cm (T_{em}), the temperatures on outer target plate (T_{ed1} – T_{ed7}) and on inner target plate (T_{ed8} – T_{ed14}) for shot 1906. This discharge first starts by limiter configuration, then divertor configuration is formed after the multipole field coils are powered. The divertor plasma is first observed on the outer divertor target at about 88ms, as shown in the T_{ed7}. It scans a 6cm distance on the neutralization plate within 20ms, the scan speed of divertor plasma is 3m/s. The SOL plasma arrives at inner target plate at about 105 ms, as shown in T_{ed14}. It begins to be detected in the T_{ed8} after 25 ms. The peak temperature on outer target plate is higher than that on inner target plate. The edge temperature of main plasma (T_{em}) drops dramatically during the divertor discharge.

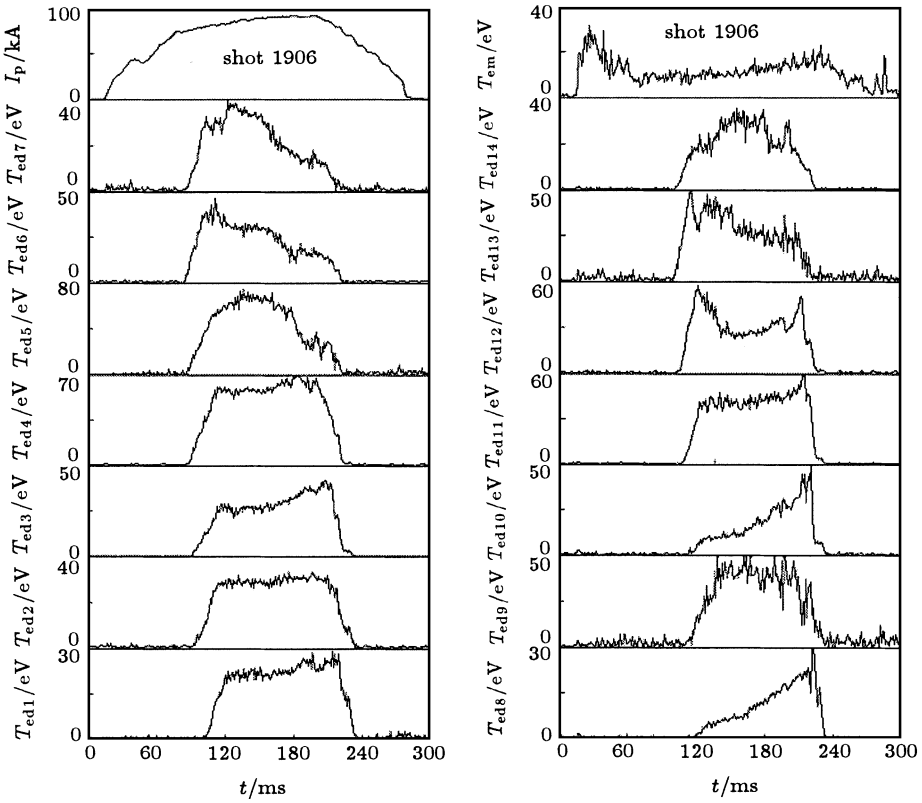


Fig.8. The time evolutions for divertor discharge parameters in shot 1906. I_p is the plasma current, T_{em} is electron temperature at a midplane radius of r=40cm, $T_{ed1} - T_{ed7}$ are electron temperatures on outer target plate, $T_{ed8} - T_{ed14}$ are electron temperatures on inner one.

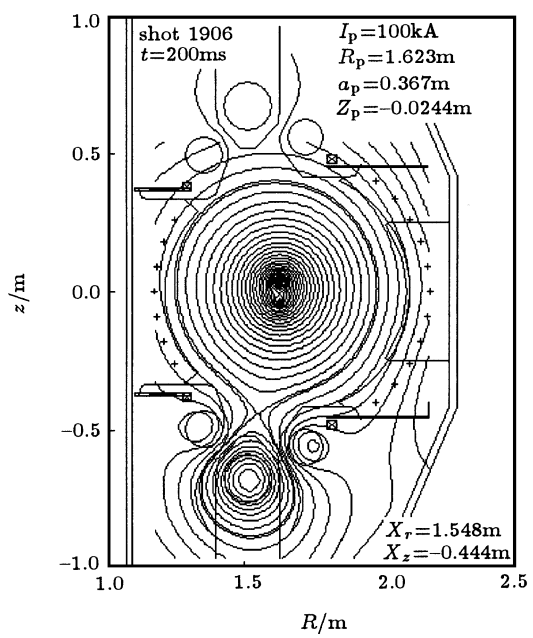


Fig.9. The divertor configuration reconstructed from the signals of 18 magnetic coils for shot 1906.

The magnetic separatrix and X-point position have been obtained from an equilibrium reconstruction code using the signals of 18 Mirnov coils. The reconstructed magnetic surface at t=200 ms for shot 1906 is shown in Fig.9. It also indicates that the divertor plasma impacts the outer target and inner one. The plasma minor radius is only 36.7cm, which means that the midplane temperature T_{em} at r=40cm should be very low, as shown in Fig.8. The plasma positions obtained by reconstruction method, such as major or minor radius and X-point are consistent with the predictions from MHD simulation code. The duration of divertor discharge determined by the reconstruction fully corresponds to that measured by probes on the neutralization plate (in Fig.8). Meanwhile, these results are also verified by those from other diagnostics, for example, vacuum ultraviolet radiation, visible light emission and neutral-gas pressure measured by a fast ionization gauge working in strong magnetic field.

Figure 10 presents the parameter evolutions of shot 1766 for plasma current I_p, the line-averaged density n_e (0), O VI, C III and H_α emissions from main vacuum chamber, $H_{\alpha,div}$ and C III-div emissions from divertor chamber, electron temperature T_{ed} and density N_{ed} on the outer target plate, line-averaged density n_{ed} measured by an 8-mm microwave interferometer, and neutralization gas pressure P in the divertor chamber. The intensities of O VI, C III and H_α emissions decrease in bulk plasma while the neutral gas

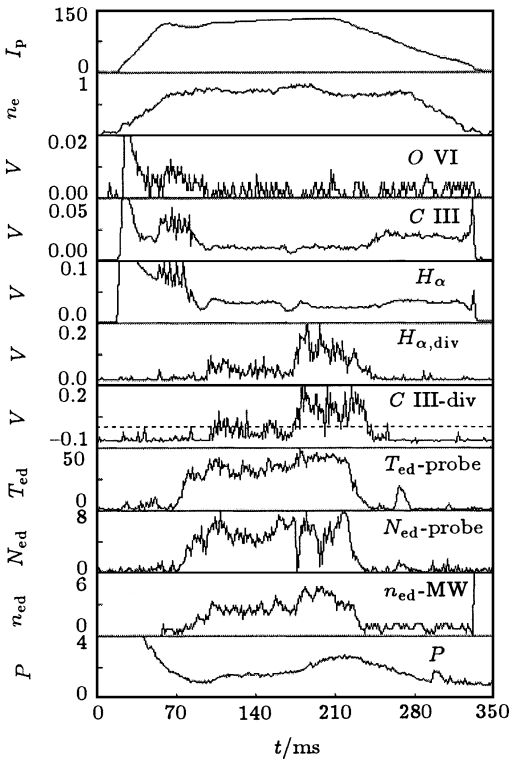


Fig.10. Time evolutions of main parameters during divertor discharge for shot 1766: Plasma current I_p(/kA), the line-averaged density n_e (0)(/10^{19}m^{-3}), OVI, C III and H_α emissions (/arb.units) from main vacuum chamber, $H_{\alpha,div}$ and C III-div emissions (/arb.units) from divertor chamber, electron temperature T_{ed}(/eV) and density N_{ed}(10^{17}m^{-3}) on the outer target plate, line-averaged electron density n_{ed}(10^{17}m^{-3}) measured by an 8-mm microwave interferometer and neutralization gas pressure P(10^{-3}Pa) measured with fast ionization gauge in the outer divertor chamber.

pressure P increases in the divertor chamber during divertor discharges. The reductions in H_α, O VI and C III intensities for bulk plasma illuminate that the edge particle recycling and the impurity flux decrease. The line-averaged density in divertor chamber (n_{ed}) measured by an 8-mm microwave interferometer is basically consistent with the density measured by the probe (N_{ed}). Neutral gas pressure P increases by one order during the divertor discharge. Its formation time is about 18ms, which is 14 ms later than that of temperature and density in the divertor chamber. The time constant of dumping the divertor particles is about 40 ms for the HL-2A vacuum system. It provides parameter important to investigation of the removal efficiency of fusion products in the HL-2A tokamak.

4. Conclusions

The experimental result in HL-2A indicates that the radial gradient of Reynolds stress induced by edge plasma turbulence can generate the edge poloidal flow. The edge electron temperature and density for divertor discharge is about 40% higher than that for limiter discharge. The decay length of electron temperature on the divertor target plate is larger than 2 cm. The electron temperature on the outer target plate is higher than that on the inner target plate. The plasma scan speed on the divertor plate is about 3 m/s. In the operation mode of divertor discharge in HL-2A, the edge plasma recycling and the impurity flux in bulk plasma decrease. The production time of the neutralization gas pressure in divertor chamber and the time constant of dumping the divertor particles are about 14ms and 40ms, respectively. They provide parameters important to the investigation of the removal efficiency of fusion productions in the HL-2A tokamak. The plasma parameters attained by magnetic surface reconstruction, such as minor radius and X-point position, accord with those predictions by MHD equilibrium code. The divertor configuration is more effective than limiter configuration to control discharge density and to reduce impurities.

References

[1] Guo H Y, Matthews G F, Coffey I, Erents S K, Groth M, Harbour P J, Hellermann M G, Hillis D L, Hogan J T, Horton L D, Ingesson L C, Lawson K D, Lingertat J, Maggi C F, McCracken G M and Monk R D 2000 *Nucl. Fusion* **40** 379

[2] Tsois N, Kyriakakis G, Kakoulidis E, Carlson A, Neuhauser J, Feneberg W and the ASDEX team 1990 *17th EPS* **14B**(3) 71

[3] Haas G, Gernhardt J, Keilhacker M, Jackson G L and Mangi R 1984 *J. Nucl. Mater.* **121** 151

[4] Tsois N, Bessenrodt W M, Carlson A, Haas G, McCormick K, Neuhauser J, Siller G, Wurz H and the ASDEX team 1989 16*th EPS* **13B** (3) 907

[5] Matthews G F 1994 *Plasma Phys. Control. Fusion* **36** 1595

[6] Hong W Y, Wang E Y, Li Q, Cao J Y and Yan L W 2002 *Chin. Phys. Lett.* **19** 1643

[7] MacLatchy C S, Boucher C, Poirier D A and Gunn J P 1992 *Rev. Sci. Instrum.* **63** 3923

[8] Lin C G and Qian S J 1998 *Chin. Phys.* **7** 22

[9] Diamond P H and Kim Y B 1991 *Phys. Fluids* B **3** 1626

[10] Hong W Y, Yan L W, Wang E Y, Li Q and Qian J 2005 *Acta Phys. Sin.* **54** 173 (in Chinese)

[11] Li G, Bengtson R D, Lin H, Meier M A, Tsui H Y W and Wootton A T 1994 *Nucl. Fusion* **34** 659

[12] Ritz C P, Powers E J, Rhodes T L, Bengtson R D and Gentle K W 1988 *Rev. Sci. Instrum.* **59** 1739